optica

Coherent random walks in free space

Toni Eichelkraut,[1] Christian Vetter,[1] Armando Perez-Leija,[1] Hector Moya-Cessa,[2] Demetrios N. Christodoulides,[3] and Alexander Szameit[1,*]

[1]Institute of Applied Physics, Friedrich-Schiller-Universität Jena, Max-Wien-Platz 1, 07743 Jena, Germany

[2]Instituto Nacional de Astrofsica, Optica y Electronica, Coordinacion de Optica, Luis Enrique Erro No. 1, 72840 Tonantzintla, Puebla, Mexico

[3]CREOL, The College of Optics and Photonics, University of Central Florida, Orlando, Florida 32816, USA

*Corresponding author: alexander.szameit@uni-jena.de

Received 16 July 2014; revised 1 September 2014; accepted 15 September 2014 (Doc. ID 216859); published 17 October 2014

Two-dimensional continuous time quantum random walks (CTQRW) are physical processes where quantum particles simultaneously evolve in different permissible directions within discrete graphs. In order to force the quantum walkers (QWs) to evolve in such a fashion, one generally requires periodic potentials. Here, we demonstrate that two-dimensional CTQRW can be generated in free space by properly tailoring the initial wave functions. We analytically show that within a certain spatial region the arising probability distribution quantitatively resembles the probability pattern exhibited by a QW traversing a periodic lattice potential. These theoretical predictions were experimentally verified using classical laser light, appropriately shaped by a spatial light modulator. Expanding the presented results to the case of multiple walkers may open new possibilities in quantum information technology using bulk optics.

OCIS codes: (270.0270) Quantum optics; (270.1670) Coherent optical effects.

http://dx.doi.org/10.1364/OPTICA.1.000268

Classical random walks are ubiquitous in various research fields such as physics, biology, and finance theory [1–4]. In most of these disciplines, classical random walks are among the most powerful mathematical tools used for developing advanced algorithms [3]. Within the framework of quantum mechanics, where the inherent superposition principle and entanglement enable parallelization, random walks of quantum particles may surpass the potential offered by their classical counterpart [5–7]. In that vein, for instance, computational algorithms based on quantum random walks have been presented to overcome several fundamental problems more efficiently [8].

In essence, one-dimensional (1D) continuous time quantum random walks (CTQRWs) can be implemented via tunneling of quantum particles between adjacent sites in discrete systems [9]. In other words, the wave dynamics occurring in coupled systems, such as crystalline structures and periodic photonic lattices, is essentially equivalent to quantum walks of single particles [2,6,10]. In fact, CTQRWs have been demonstrated using different physical platforms ranging from nuclear magnetic resonance [11] and optical resonators [12] to evanescently coupled waveguide lattices [13]. Additionally, an approach to extend the concept of CTQRWs to some other physical setting where the so-called quantum walkers (QWs) can freely evolve might be of interest. That is, provided the fact that such free evolution—in the absence of any external potential—would exhibit a dynamical behavior comparable to a CTQRW.

In this Letter, we demonstrate that CTQRWs can be realized in free space through the spatial evolution of a single QW whose initial wave function ψ is appropriately shaped so as to exhibit the highest probability amplitude around the origin. We experimentally demonstrate our theoretical findings by using paraxial optical beams. Evidently, the usage of such classical beams to explore the propagation dynamics of point-like quantum particles is possible since both phenomena are mathematically described by the same equation. This, in turn, makes our approach suitable for the realization of random walks using different quantum particles, including electrons and single photons [14]. For instance, the feasibility of tailoring electron wave packets is by now possible employing nanoscale holograms [15].

Since the terms quantum random walk and coherent random walk can be used synonymously [6], and because our experiments were conducted using classical light, throughout our Letter we refer to coherent random walks (CRWs). To study the spatial evolution of a general wave function envelope $\psi(x, y, z)$, we consider the paraxial wave equation

$$\left(i\frac{\partial}{\partial z}+\frac{1}{2k}\nabla_{\perp}^{2}\right)\psi=0, \tag{1}$$

which can be derived from first principles for both quantum particles and light beams. Here, we use $\nabla_{\perp}^{2}=\partial^{2}/\partial x^{2}+\partial^{2}/\partial y^{2}$; z is the propagation distance and $k=2\pi/\lambda$ is the wave number. As previously mentioned, the evolution of quantum particles and classical light follows the same mathematical description. Thus, Eq. (1) is equivalent to the Schrödinger equation, which describes the temporal evolution of free particles. In fact, the temporal evolution can also be mapped to a spatial propagation; for instance, this formalism has been successfully used in Ref. [15] to study the generation of electron Airy beams.

We start our analysis with the initially *localized* wave function envelope

$$\psi(x,y,0)=N\mathrm{e}^{-(x^{2}+y^{2})/2\sigma^{2}}J_{n}(\alpha x)J_{n}(\alpha y), \tag{2}$$

which is symmetric around the origin ($x=y=0$), and $J_n(\alpha x)$ represents a Bessel function of the first kind of order n. Note that the Gaussian apodization guarantees the requirement of finite energy, while N provides the necessary normalization. Importantly, the Bessel profiles introduced here are not azimuthally symmetric as the usual diffraction-free Bessel beams. Following the approach reported in Refs. [16,17], one can show that the evolution dynamics of such initially Gaussian-apodized Bessel envelopes is analytically described by

$$\psi(x,y,z)=N\prod_{s\in\{x,y\}}\left(1-\frac{iz}{k\sigma^{2}}\right)^{-1/2}\exp\left[\frac{-2ks^{2}+i\alpha^{2}\sigma^{2}z}{4(k\sigma^{2}-iz)}\right]\times\sum_{l=-\infty}^{\infty}(-i)^{l}J_{n+2l}(A(s,z))J_{l}(B(z)). \tag{3}$$

Here, we have $A(s,z)=\alpha k\sigma^{2}s/(k\sigma^{2}-iz)$ and $B(z)=\alpha^{2}(z+iz^{2}/(k\sigma^{2}-iz))/(4k)$, with s taking the place of x and y, respectively.

Of particular interest for our work is the case where the initial probability amplitude is given by

$$\psi(x,0)=N\exp[-x^{2}/2\sigma^{2}]J_{0}(\alpha x). \tag{4}$$

In this 1D scenario, the arising probability distribution within a parabolic region in the (x,z) plane (depicted in Fig. 1) resembles not only qualitatively but quantitatively [18] the probability pattern exhibited by a QW traversing a uniform periodic potential [9,13]. This is true, despite the fact that the evolution takes place in free space, i.e., a lattice potential is not present at all.

In order to analytically derive the evolution dynamics of the initial wave function as given in Eq. (4), we consider the case of a very broad Gaussian envelope ($k\sigma^{2}\gg z;\sigma\gg x$) apodizing a Bessel profile of order zero, as given in Eq. (4), such that the evolution dynamics can be approximated by

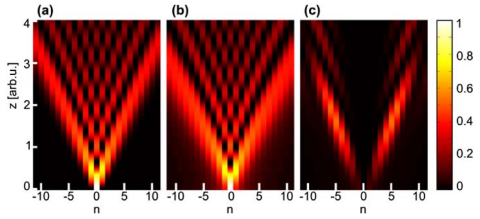

Fig. 1. Theoretical probability evolution. (a) Probability distribution $|\psi_{\mathrm{lattice}}(n,z)|^{2}$ expected for a quantum walker traversing a uniform lattice, where the lattice sites are labeled by n. (b) Calculated free space probability density, $|\psi_{\mathrm{fs}}(x_n,z)|^{2}$, plotted for the different transverse positions $x_n=n\pi/\alpha$. (c) The difference $|\psi_{\mathrm{fs}}(x_n,z)-\psi_{\mathrm{lattice}}(n,z)|^{2}$.

$$\psi(x,z)=\sum_{l=-\infty}^{\infty}(-i)^{l}J_{2l}(\alpha x)J_{l}\left(\frac{\alpha^{2}z}{4k}\right). \tag{5}$$

Note that Eq. (5) is only valid within a finite transverse window and for a certain propagation distance, both determined by the apodization envelope ($k\sigma^{2}\gg z;\sigma\gg x$). From Eq. (5), one can readily see that at $x=0$, the evolution is simply given by $\psi(x=0,z)=J_{0}(\alpha^{2}z/4k)$, which is identical to the probability amplitude of a single QW in the excited site of a uniform lattice [10,13]. Furthermore, for every $x_m=m\pi/\alpha$, m being an integer, one can show [18] that the evolution equation Eq. (5) becomes

$$\psi(x_m,z)=(-i)^{m}J_{m}(\alpha^{2}z/4k), \tag{6}$$

which is mathematically identical to the probability amplitude described by a QW along the mth site within a periodic lattice [10,13]. To be precise, Eq. (6) is a good approximation within the aforementioned parabolic region bounded by $z>z_m\approx 16k(m^{2}+2m+1)/\alpha^{2}$ [18].

In Fig. 1, we illustrate these effects by comparing the probability pattern of a QW traversing a periodic potential, given by Eq. (6), and the probability distribution corresponding to a single QW propagating in free space described by Eq. (5). In order to have a meaningful comparison between $|\psi_{\mathrm{lattice}}(n,z)|^{2}$ and $|\psi_{\mathrm{fs}}(x_n,z)|^{2}$, it is important to be aware of the fact that $|\psi_{\mathrm{lattice}}(n,z)|^{2}$ is a probability distribution, whereas $|\psi_{\mathrm{fs}}(x,z)|^{2}$ is a probability density. Consequently, in Fig. 1, we actually plot $\int_{x_n-\Delta x/2}^{x_n+\Delta x/2}|\psi_{\mathrm{fs}}(x,z)|^{2}\mathrm{d}x\approx|\psi_{\mathrm{fs}}(x_n,z)|^{2}\Delta x$, where we integrate over a very small transverse distance. For brevity, we omitted the Δx in the caption of Fig. 1. Note that in an experiment, the transverse width Δx is associated with the detector width. Figure 1(c) depicts the difference between both space-evolved wave functions, $|\psi_{\mathrm{fs}}-\psi_{\mathrm{lattice}}|^{2}$. It is well perceived that within the specified region the deviation between both propagation patterns, which includes their respective phases, is almost negligible.

In order to experimentally verify our theoretical findings, we have shaped the amplitude and phase of a collimated light beam using a spatial light modulator (SLM). The corresponding setup is shown in Fig. 2. In order to generate the desired input field in the $z=0$ plane, we implement its Fourier transform $\tilde{\psi}(\xi,\eta)=\mathrm{FT}[\psi]$ on the SLM. In general, the field at the SLM plane can be written as $\tilde{\psi}(\xi,\eta)=M(\xi,\eta)\exp[i\phi(\xi,\eta)]$,

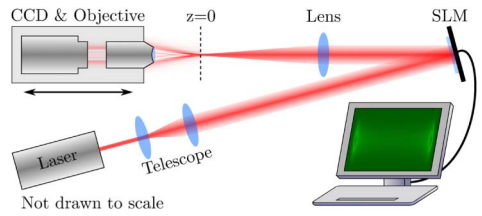

Fig. 2. Experimental setup consisting of a Helium Neon laser ($\lambda = 633$ nm), telescope for beam expansion, spatial light modulator (Holoeye Pluto VIS) for amplitude and phase modulation, spherical lens ($f = 300$ mm) for Fourier transformation, microscope objective (10× Olympus Plan Achromat) for imaging, and movable CCD camera (Basler Ace 1600-20gm).

where $M(\xi,\eta)$ and $\phi(\xi,\eta)$ represent the amplitude and phase distribution, respectively. Following [19], any complex function, such as $\tilde{\psi}(\xi,\eta)$, can be obtained by applying a phase-only modulation given by

$$\chi(\xi,\eta) = \exp[iM(\xi,\eta)[\phi(\xi,\eta) + \phi_G(\xi,\eta)]]. \quad (7)$$

Importantly, the imposed periodic phase $\phi_G(\xi,\eta) = 2\pi(\xi,\eta)/d$ acts as a grating that separates the different diffraction orders. When Fourier transforming the beam using a spherical lens and postselecting the first diffraction order, the desired field distribution is obtained at $z = 0$. In our case, we set $d = 64$ μm and the focal length of the lens to $f = 300$ mm. The three-dimensional intensity distribution of the light was recorded using a 10× microscope objective and a CCD camera mounted on a movable linear stage. The propagation distance under study was chosen to be $\Delta z = 2.5$ cm.

For the creation of a 1D free space CRW, we generate the initial field distribution given by Eq. (4) with $\alpha = 125$ mm^{-1} and $\sigma = 0.13$ mm. The experimental propagation pattern over the (x, z) plane is shown in Fig. 3(b) along with the actual camera images of the intensity distribution at $z = 0$ cm and $z = 2.5$ cm on bottom and top, respectively. Note the good agreement between the experimental data, Fig. 3(b), and our theoretical predictions, Fig. 3(a). This is possible since for the chosen experimental parameters, $\sigma = 0.13$ mm, the propagation distance under consideration falls within the established limits, that is, $z \ll k\sigma^2$ and $k\sigma^2 = 18$ cm. To quantitatively assess the agreement between the observed and the theoretically expected results, in Fig. 3 we superimpose both intensity patterns. Figure 3(c) depicts the intensity distribution in the initial plane for $y = 0$. The intensity contrast between the central maximum and the first side minimum, for instance, is $I_{max}/I_{min} \approx 143$, whereas no emphasis has been laid on maximizing this ratio. Moreover, to fully quantify the agreement between theory and experiment, we calculated the coefficient of determination which, for the values depicted in Fig. 3(c), is $R^2 = 0.9915$. Figure 3(d) shows the longitudinal intensity distribution along z at $x_0 = 0$ and $x_1 = \pi/\alpha \approx 25$ μm, as well as the theoretically predicted Bessel patterns. From this graph one can clearly see that the most pronounced difference between the experimentally observed evolution and the Bessel pattern is found at x_1 for $z \approx 0$ whereas, for larger propagation distances, the deviation decreases.

We would like to emphasize that single-photon CRWs can be realized in our setup by replacing the continuous wave laser with a single-photon source and scanning the transverse position x_m using photon-counting detectors.

Another interesting scenario occurs when a linear superposition of two transverse Bessel profiles of order zero, $\psi(x, 0) = \exp[-x^2/2\sigma^2](J_0(\alpha x) + J_0(\alpha x - n\pi))$, is considered as initial wave envelope. In this case, the arising probability distribution corresponds to a situation where a single QW is initially prepared in a coherent superposition of states. In this setting, the initial wave function features two main lobes separated by a transverse distance of $\Delta x = n\pi/\alpha$. In Fig. 4, this process is depicted for the specific case of $n = 2$. In addition, in [18], it is shown that within a certain region the dynamics obeyed by the QW propagating in free space is indeed identical to the one exhibited by a QW being simultaneously launched into two sites of a periodic lattice. The experimental results presented in Fig. 4(b) were obtained analogously to the single excitation case.

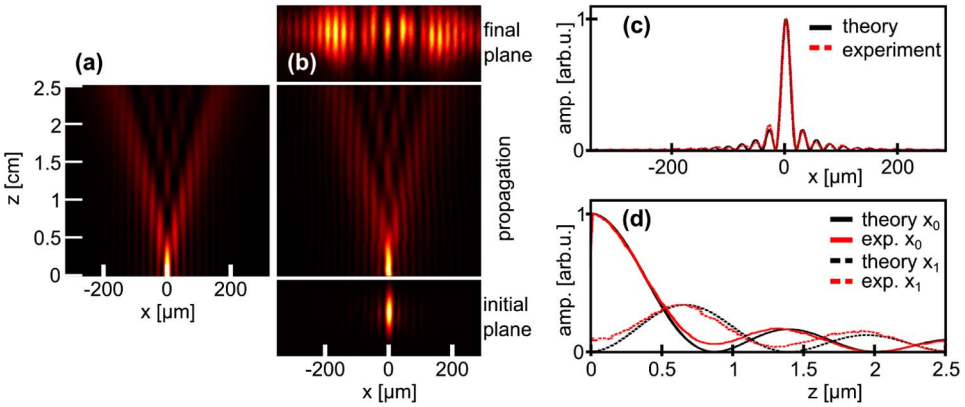

Fig. 3. Theoretical and experimental comparison for a 1D CRW in free space. (a) Theoretical free-space probability evolution corresponding to the initial wave profile given by Eq. (4) using the parameters $\alpha = 125$ mm^{-1} and $\sigma = 0.13$ mm. (b) Bottom, experimental intensity envelope as produced in our setup at $z = 0$ cm. Center, recorded intensity evolution of the light beam at the plane $y = 0$. Top, final intensity pattern after a propagation distance of $z = 2.5$ cm. (c) Comparison between theoretical and experimental intensity distribution in the initial plane at $y = 0$. (d) Comparison between theoretical and experimental intensity evolution at two different transverse positions. $x_0 = 0$ and $x_1 = \pi/\alpha \approx 25$ μm.

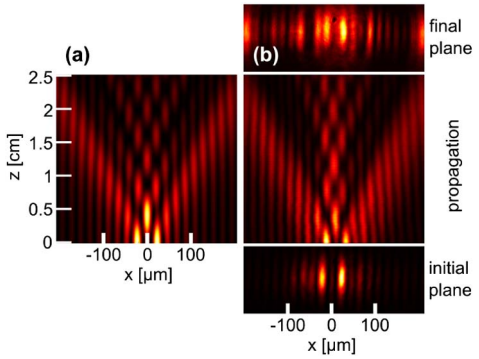

Fig. 4. Theoretical and experimental comparison for a 1D CRW in a coherent superposition of states. (a) Theoretical free-space probability evolution of the initial wave function $\psi(x,0) = \exp[-x^2/2\sigma^2](J_0(\alpha x) + J_0(\alpha x - 2\pi))$ using the parameters $\alpha = 145\ \mathrm{mm}^{-1}$ and $\sigma = 1$ mm. (b) Bottom, experimental initial intensity profile. Center, top view of the intensity evolution. Top, intensity pattern recorded after a propagation distance of $z = 2.5$ cm.

Finally, in order to demonstrate the potentiality of this approach for the realization of 2D free space CRWs, we consider the experimental propagation of the initial field profile given by

$$\psi(x,y,0) = \exp[-(x^2+y^2)/2\sigma^2]J_0(\alpha x)J_0(\alpha y). \quad (8)$$

To do so, we tune the SLM such that $\alpha = 310\ \mathrm{mm}^{-1}$ and $\sigma = 0.13$ mm. The experimental propagation dynamics are presented in Fig. 5, where now the intensity pattern resembles the probability distribution of a QW evolving through a 2D square lattice. Figures 5(a)–5(c) show the experimental intensity patterns registered at three planes perpendicular to the propagation direction. These observations fully confirm our theoretical predictions depicted in Figs. 5(d)–5(f). The

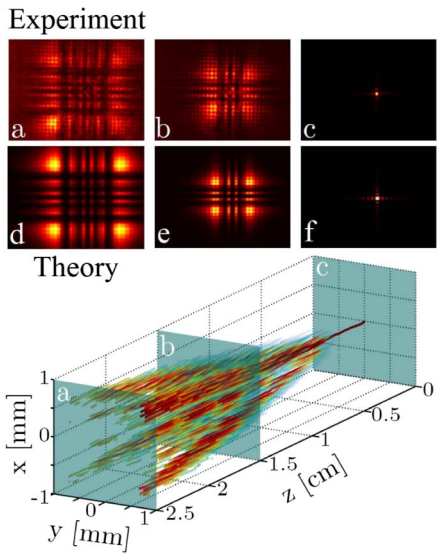

Fig. 5. Experimental results for a 2D CRW. Top row, experimental images taken with a CCD camera. Central row, theoretical intensity evolution. Bottom row, stitched image from all camera images, showing the 2D CRW of a "single excitation."

3D picture at the bottom of Fig. 5 shows the experimental evolution of the registered light spots where the intensity is a local maximum. We emphasize again that the evolution takes place in free space and no lattice potential is present.

In conclusion, we have demonstrated theoretically and experimentally that CRWs can be generated in the absence of any periodic environment, e.g., in the bulk of a uniform material or even in free space. We performed experiments using classical light beams that resemble a probability distribution of QWs as if a lattice potential were present. With current technology, we foresee that experiments will soon be feasible using real quantum particles, in particular photons and electrons (see, e.g., [15]). As CTQRWs carry the potential of substantially accelerating computation schemes [2,8], our results may open new possibilities in quantum information technology using bulk optics. However, this potential can only be fully tapped by expanding the presented results to the case of multiple walkers.

FUNDING INFORMATION

Deutsche Forschungsgemeinschaft (DFG) (NO462/6-1); German Ministry of Education (ZIK 03Z1HN31); German-Israeli Foundation for Scientific Research and Development (GIF) (1157-127.14/2011); Thuringian Ministry for Education, Science and Culture (11027-514).

See Supplement 1 for supporting content.

REFERENCES AND NOTES

1. Y. Aharonov, L. Davidovich, and N. Zagury, Phys. Rev. A **48**, 1687 (1993).
2. J. Kempe, Contemp. Phys. **44**, 307 (2003).
3. V. M. Kendon, Phil. Trans. R. Soc. A **364**, 3407 (2006).
4. P. L. Knight, E. Roldán, and J. E. Sipe, Phys. Rev. A **68**, 020301 (2003).
5. A. M. Childs, Phys. Rev. Lett. **102**, 180501 (2009).
6. O. Mulken and A. Blumen, Phys. Rep. **502**, 37 (2011).
7. T. Kitagawa, M. A. Broome, A. Fedrizzi, M. S. Rudner, E. Berg, I. Kassal, A. Aspuru-Guzik, E. Demler, and A. G. White, Nat. Commun. **3**, 882 (2012).
8. P. W. Shor, SIAM J. Comput. **26**, 1484 (1997).
9. H. B. Perets, Y. Lahini, F. Pozzi, M. Sorel, R. Morandotti, and Y. Silberberg, Phys. Rev. Lett. **100**, 170506 (2008).
10. Y. Bromberg, Y. Lahini, R. Morandotti, and Y. Silberberg, Phys. Rev. Lett. **102**, 253904 (2009).
11. J. A. Jones, Prog. Nucl. Magn. Reson. Spectrosc. **59**, 91 (2011).
12. D. Bouwmeester, I. Marzoli, G. P. Karman, W. Schleich, and J. P. Woerdman, Phys. Rev. A **61**, 013410 (1999).
13. A. Peruzzo, M. Lobino, J. C. F. Matthews, N. Matsuda, A. Politi, K. Poulios, X.-Q. Zhou, Y. Lahini, N. Ismail, K. Woerhoff, Y. Bromberg, Y. Silberberg, M. G. Thompson, and J. L. O'Brien, Science **329**, 1500 (2010).
14. J. E. Sipe, Phys. Rev. A **52**, 1875 (1995).
15. N. Voloch-Bloch, Y. Lereah, Y. Lilach, A. Gover, and A. Arie, Nature **494**, 331 (2013).
16. A. Perez-Leija, F. Soto-Eguibar, S. Chavez-Cerda, A. Szameit, H. Moya-Cessa, and D. N. Christodoulides, Opt. Express **21**, 17951 (2013).
17. G. Dattoli and A. Torre, J. Opt. Soc. Am. B **31**, 2214 (2014).
18. See Supplement 1 for a complete rigorous analysis.
19. J. A. Davis, D. M. Cottrell, J. Campos, M. J. Yzuel, and I. Moreno, Appl. Opt. **38**, 5004 (1999).